Epitaxy of $(GaN)_{1-x}(ZnO)_x$ Solid-Solution Thin Films with Widely Tunable Chemical Composition and Strong Visible Absorption

Chang Yang,[1,2,3,*] Yasushi Hirose,[1,2,†] Takuto Wakasugi,[1] Naoki Kashiwa,[1] Hiroki Kawai,[4,5] Koichi Yamashita,[4] and Tetsuya Hasegawa[1,2]

[1] *Department of Chemistry, The University of Tokyo, Bunkyo-ku, Tokyo 113-0033, Japan*
[2] *Kanagawa Academy of Science and Technology (KAST), Kawasaki 213-0012, Japan*
[3] *Felix-Bloch-Institut für Festkörperphysik, Universität Leipzig, Linnéstr. 5, 04103 Leipzig, Germany*
[4] *Department of Chemical System Engineering, The University of Tokyo, Bunkyo-ku, Tokyo 113-0033, Japan*
[5] *Institute of Memory Technology Research & Development, Toshiba Memory Corporation, 1-1, Shibaura 1-chome, Minato-ku, Tokyo 105-8001, Japan*

(Received 14 November 2017; revised manuscript received 26 April 2018; published 1 October 2018)

The alloying of wide-band-gap ZnO and GaN causes band-gap reduction, enabling visible-light-driven photocatalysis for high-efficiency water splitting. However, challenges in single-crystal $(GaN)_{1-x}(ZnO)_x$ solid-solution synthesis prevent a better understanding of the optical properties and electronic structures. Here, low-temperature epitaxial growth of $(GaN)_{1-x}(ZnO)_x$ thin films with a wide tunability of chemical composition is demonstrated by using a multitarget pulsed-laser-deposition (PLD) system. The phase pure $(GaN)_{1-x}(ZnO)_x$ solid solution is obtained by alternately depositing GaN and ZnO with the thickness of each GaN/ZnO pair set within one or two unit cells. The band gap of the solid-solution thin films as a function of systematically controlled chemical composition shows asymmetric bowing with a minimum at approximately 2.0 eV for $x = 0.65$. Furthermore, a large absorption coefficient ($>10^4$ cm^{-1}) in the visible-light region is observed. The shape of the absorption edge is not consistent with that of a direct-transition semiconductor. First-principles calculation suggests that this inconsistency originates from localization of the valence-band maximum on N atoms bonded with Zn. A technique for fabricating high-quality epitaxial $(GaN)_{1-x}(ZnO)_x$ solid solutions is essential for acquiring a deep understanding of the fundamental properties of this system.

DOI: 10.1103/PhysRevApplied.10.044001

I. INTRODUCTION

Photocatalytic solar water splitting using semiconductors is a promising way to generate clean and sustainable hydrogen energy [1,2]. However, the solar to hydrogen conversion efficiency is too low to be practical. To improve the efficiency, the development of a semiconductor photocatalyst with a high visible-light activity is crucial. In 2005, Maeda *et al.* achieved visible-light-driven photocatalytic water splitting with a $(GaN)_{1-x}(ZnO)_x$ solid solution [3,4]. Because the hydrogen conversion efficiency of $(GaN)_{1-x}(ZnO)_x$ under visible light was much higher than those of conventional oxide photocatalysts [3–6], the discovery has triggered studies of these (oxy)nitrides [7–10].

An intriguing feature of $(GaN)_{1-x}(ZnO)_x$ is that alloying of the wide-band-gap ZnO and GaN reduces the band gap [3–6,10–17]. For $(GaN)_{1-x}(ZnO)_x$ nanocrystals with a wide compositional range, the absorption onset energy can be reduced to 2.2 eV for a ZnO-rich composition [15,18]. The mechanism of this bandgap narrowing is, however, still under debate. Possible causes include N 2*p* and Zn 3*d* repulsion [8,19,20], localized Zn acceptor levels [21,22], short-range local order [7], or repulsion of the conduction-band edges of GaN and ZnO phases [23].

This controversy stems from the fact that the fundamental optical properties of $(GaN)_{1-x}(ZnO)_x$ have not been fully established experimentally. For example, there is a large distribution of the estimated absorption onset energy (See Supplemental Material [24], Fig. S1). Furthermore, the absorption coefficient, which is one of the most essential parameters of a photocatalytic material, was reported only for colloidal solutions of nanocrystals with a specific composition of $(GaN)_{0.27}(ZnO)_{0.73}$ [25]. These problems are the result of the synthetic process. $(GaN)_{1-x}(ZnO)_x$ is usually synthesized in a fine powder or nanocrystalline form via ammonolysis or combustion [3–6,10–17,26–31]. Hence, their optical properties have been evaluated by diffuse reflectance spectroscopy (DRS). Although DRS is a well-established technique to investigate the optical properties of a powder sample, it has the

*yangchangyc@gmail.com
†hirose@chem.s.u-tokyo.ac.jp

 © 2018 American Physical Society

following limitations: (1) The spectral shape is hindered by differences in the scattering factor between the sample and a standard [32]; and (2) the absorption spectrum calculated from DRS does not yield absolute absorption coefficients. Therefore, deeper investigations into the band-gap narrowing of $(GaN)_{1-x}(ZnO)_x$ will require bulk single crystals or thin films to enable conventional optical transmittance and/or reflectance measurements.

Despite extensive studies of $(GaN)_{1-x}(ZnO)_x$, thin-film synthesis has rarely been reported [33,34]. Furthermore, the chemical compositions were not evaluated in previous studies where polycrystalline thin films were fabricated by reactive rf magnetron sputtering. Here, we demonstrate epitaxial growth of $(GaN)_{1-x}(ZnO)_x$ solid solutions with a wide range of chemical compositions by using pulsed laser deposition (PLD). The solid-solution films exhibit strong visible-light absorption, with coefficients on the order of 10^4 cm^{-1}. Spectral shapes of the absorption edges exhibit poor agreement with the Tauc plots that assume a direct transition, which has been used in previous studies. Theoretical calculation suggests that this is due to the flat valence-band top caused by the orbital localization on N atoms bonded with Zn. The energy of the absorption edge E_g depends on the chemical composition x, where the lowest $E_g \sim 2.0$ eV is obtained at $x = 0.65$.

II. EXPERIMENT

$(GaN)_{1-x}(ZnO)_x$ thin films are fabricated on atomically flat (0001) planes of α-Al_2O_3 and ZnO substrates by alternately depositing ZnO and GaN with multitarget PLD. Ceramic ZnO pellet and liquid Ga targets are ablated for deposition of ZnO and GaN, respectively. Figure 1(a) shows the timing chart for the multitarget PLD. Each ZnO or GaN target is synchronized with a 248-nm, 2-Hz KrF excimer laser, a variable laser attenuator (0.5 J-cm^{-2} pulse^{-1} for ZnO and 2.0 J-cm^{-2} pulse^{-1} for GaN), a piezoelectric leak valve controlling oxygen partial pressure (Oxford Applied Research, PLV-1000; $P_{O_2} = 1.0 \times 10^{-4}$ Torr for ZnO and less than 1.0×10^{-8} Torr for GaN), and an electron-cyclotron-resonance (ECR) plasma source activating nitrogen gas (Tectra, Gen2; turned on only for GaN). The partial nitrogen pressure P_{N_2} during the growth and the input current of the ECR source are 1.0×10^{-4} Torr and 40 mA, respectively.

Thicknesses of the films are determined with a stylus profiler (Veeco, Dektak 6M). Chemical compositions of the thin films are evaluated by energy dispersive x-ray spectroscopy (EDX) on a scanning electron microscope (JEOL, JSM-7100F with JED-2300). The background signal from the substrate is excluded by setting the electron accelerating voltage to 2.5 kV. The probing depth is approximately 80 nm, as estimated by Monte Carlo simulations [35]. Crystallographic structures of the thin films are characterized by x-ray diffraction (XRD) using a four-axis diffractometer with an area detector (Bruker, D8 Discover with GADDS). The out-of-plane lattice constants are calculated from (0002) diffraction of a

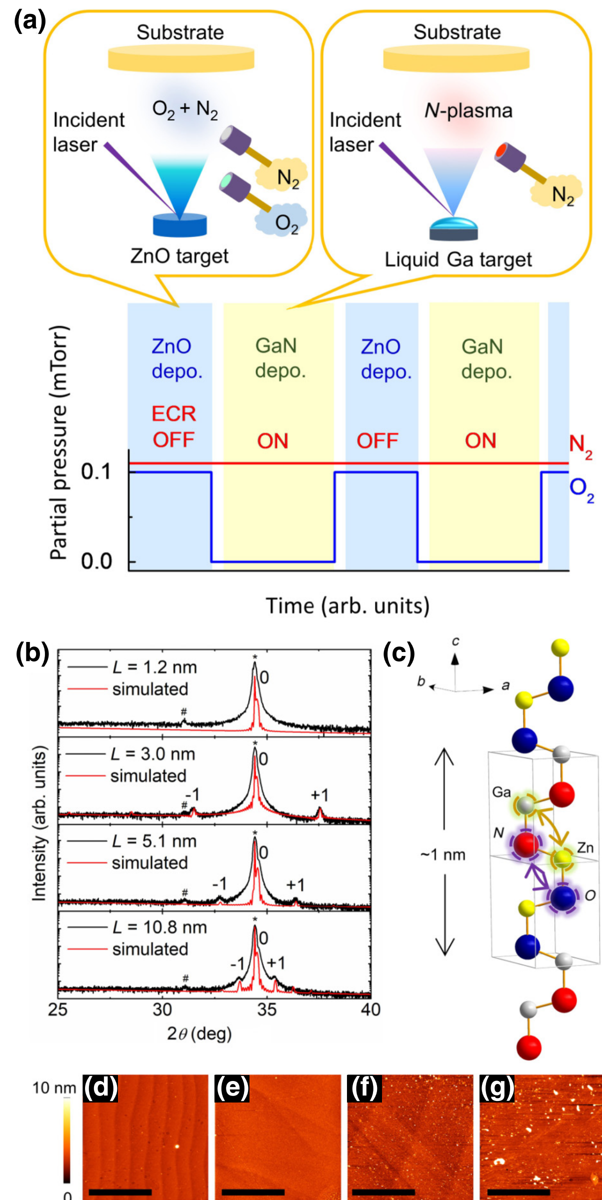

FIG. 1. (a) Schematic of the multitarget PLD system and a timing chart for periodic growth of GaN/ZnO thin films. (b) XRD θ-2θ patterns of GaN/ZnO multilayers grown on ZnO(0001) substrates with different GaN/ZnO pair thicknesses (L). The substrate peaks are marked as asterisks, and the signals from the sample holder are marked as hash signs. The superlattice main peak is denoted by 0, and the first-order satellite peaks are denoted by -1 and $+1$. (c) Schematic atomic configurations of the $1 \times 1 \times 2$ wurtzite unit cell of the GaN-ZnO solid solution with possible atom mixing at the cell interfaces. (d–g) AFM images of GaN/ZnO thin films grown on ZnO(0001) substrates with (d) $L = 1.2$ nm, (e) 3.0 nm, (f) 5.1 nm, and (g) 10.8 nm, respectively. Scale bars represent 5 μm.

wurtzite structure. The in-plane lattice constants are calculated from (1 0 –1 1) diffraction and the out-of-plane lattice constants calculated above. For (1 0 –1 1) diffraction measurements, the χ (tilt) and φ (in-plane) angles of the sample are adjusted to detect the diffraction spot on the area detector. Surface morphology of the films is evaluated using an atomic force microscope (AFM) (SII Nanotechnology, SPA400 with SPI4000). Optical transmittance T and reflectance R of the films are measured at room temperature with an ultraviolet-visible spectrometer (JASCO V-670), and optical absorbance A is calculated from $A = (1 - R - T)/(1 - R)$. The measurements are performed under regular transmittance/reflectance configuration without integration sphere, because the films are so flat that light scattering is negligible. The absorption coefficient α is evaluated from $1 - A = \exp(-\alpha\, t)$.

The density-functional-theory-based first-principles calculation is carried out for $(GaN)_{1-x}(ZnO)_x$ ($x = 0$, 0.25, 0.75, and 1) using the Vienna ab initio simulation package (VASP) [36]. For the structural optimization, the projector-augmented-wave (PAW) method [37] with the local-density-approximation (LDA) functional [38] is used with a cutoff energy of 500 eV. We also calculate the electronic structure with the LDA + U method, where U for d orbitals of Ga and Zn are set at 8.5 and 8.0 eV, respectively.

III. RESULTS AND DISCUSSION

A. Formation of epitaxial solid solutions from superlattices

$(GaN)_{1-x}(ZnO)_x$ thin films are epitaxially grown on (0001) planes of α-Al_2O_3 and ZnO substrates with a multitarget PLD system that alternately deposits ZnO and GaN. The target exchange and gas supply switching are synchronized with a pulsed KrF excimer laser, as illustrated in Fig. 1(a). The total film thickness is approximately 90 nm. Zn evaporation is suppressed at low growth temperatures, as reported for the bulk synthesis [31], by keeping the substrates below 100 °C. The $(GaN)_{1-x}(ZnO)_x$ compositions (x) are controlled by the thickness ratio of the sublayer (ZnO or GaN), allowing a wide chemical composition tunability ($x = 0.1$, 0.3, 0.5, 0.7, and 0.9). For example, the $(GaN)_{0.5}(ZnO)_{0.5}$ film is composed of GaN/ZnO pairs with the thickness ratio of 1:1 for the GaN and ZnO layers in each pair.

We first check the influence of the thickness of a GaN/ZnO pair on the crystal structure of the obtained films. Figure 1(b) shows the θ-2θ XRD patterns of the $(GaN)_{0.5}(ZnO)_{0.5}$ samples with different thicknesses of the GaN/ZnO pair from 1 to 10 nm. Owing to the good lattice matching to the substrates, all samples show the (0001) oriented epitaxial growth on ZnO(0001) substrates. When the thickness of a GaN/ZnO pair ranges from 3 to 10 nm, satellite peaks from GaN/ZnO superlattices appear. The thicknesses of the GaN/ZnO pair calculated from the positions of satellite peaks are consistent with the designed values (see Supplemental Material [24], Table S1). In contrast, satellite peaks disappear by reducing the thickness of a GaN/ZnO pair to 1.2 nm, indicating the formation of a solid solution (pseudo-alloy). Considering the fact that the 1.2-nm-thick GaN/ZnO pair includes only 4 layers of GaN and ZnO as illustrated in Fig. 1(c), the solid solution is probably formed by interlayer mixing due to the relatively high kinetic energy of the ablated atoms. AFM observations [Figs. 1(d)–1(g)] reveal that the surfaces of the solid-solution films are very smooth, indicating that the formation of the solid solution proceeds homogeneously. Based on these results, we hereafter fix the thickness of a GaN/ZnO pair at approximately 1 nm to obtain the solid-solution samples.

Subsequently, the compositional and structural properties of the $(GaN)_{1-x}(ZnO)_x$ solid solutions are investigated. Figure 2(a) plots EDX spectra of the $(GaN)_{1-x}(ZnO)_x$ thin films grown on Al_2O_3 substrates. In Fig. 2(b), the O/(N + O) and Zn/(Zn + Ga) ratios in the films, calculated

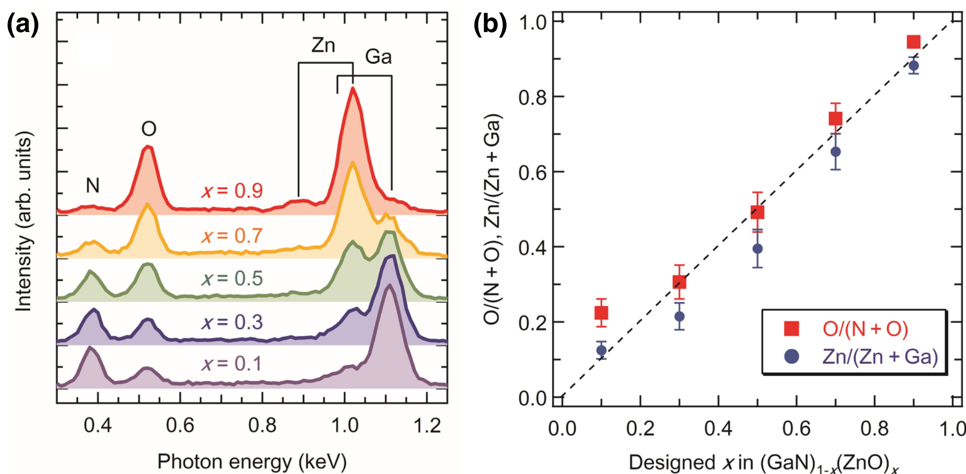

FIG. 2. (a) EDX spectra of $(GaN)_{1-x}(ZnO)_x$ thin films grown on Al_2O_3 substrates. (b) O/(N + O) and Zn/(Zn + Ga) ratios in the $(GaN)_{1-x}(ZnO)_x$ thin films calculated from the EDX spectra plotted against the designed x.

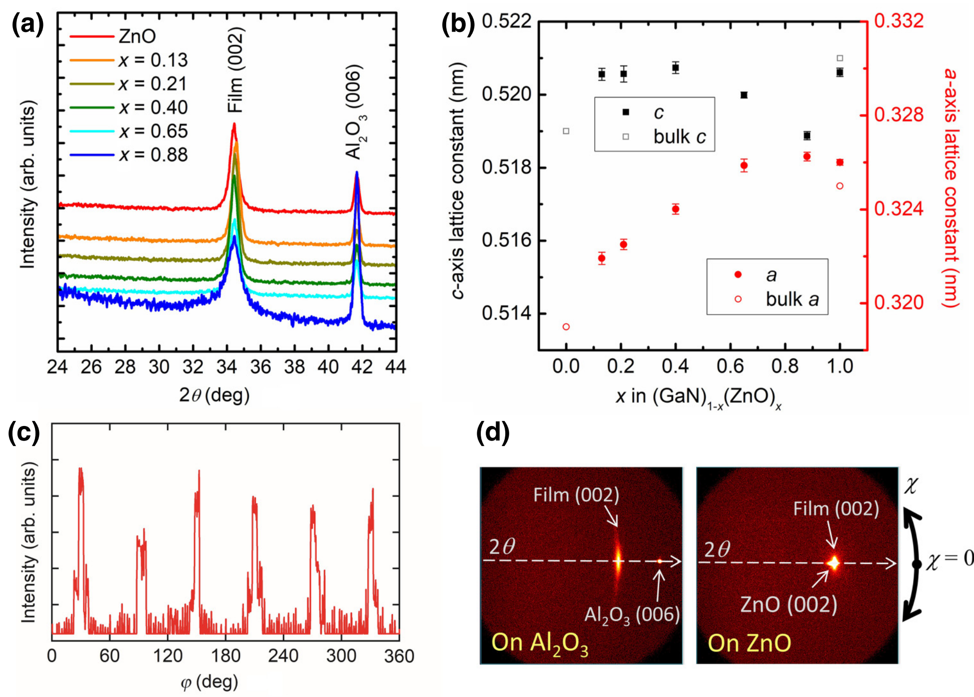

FIG. 3. (a) XRD θ-2θ patterns of $(GaN)_{1-x}(ZnO)_x$ thin films grown on Al_2O_3 substrates. (b) In-plane (a) and out-of-plane (c) lattice constants of $(GaN)_{1-x}(ZnO)_x$ thin films grown on Al_2O_3 substrates against x. (c) A φ scan plot of (1 0 –1 1) diffractions in XRD patterns of $(GaN)_{1-x}(ZnO)_x$ thin film grown on an Al_2O_3 substrate ($x = 0.65$). (d) Typical XRD two-dimensional detector images of the $(GaN)_{1-x}(ZnO)_x$ thin films on Al_2O_3 and ZnO substrates ($x = 0.65$).

from the spectra, are plotted vs x. The chemical compositions of the films almost agree with the designed values. The most Ga-rich film ($x = 0.1$) is relatively overoxidized [$O/(N + O) = 0.2$], which possibly occurs from oxidation during the period of O_2 supply before the ZnO deposition. The small deviation of the $Zn/(Zn + Ga)$ ratio from the designed value is attributable to a variation of the deposition rate, which might originate from a change of the surface state of the target due to laser ablation. In the following sections, the chemical composition of $Zn/(Zn + Ga)$ is used to distinguish samples.

Figure 3(a) shows XRD patterns of the films grown on Al_2O_3 (0001) substrates. Only (000l) diffraction peaks from a wurtzite structure are observed without impurities, such as $ZnGa_2O_4$ or Ga_2O_3, or satellite peaks from superlattices. In previous $(GaN)_{1-x}(ZnO)_x$ solid solutions, the lattice parameters monotonically increased with x [13]. Figure 3(b) plots in-plane and out-of-plane lattice constants of these films. Both lattice constants depend on x, which is generally consistent with previous data [13]. This composition-dependent change of lattice constants as well as the absence of the satellite peaks indicates that the $(GaN)_{1-x}(ZnO)_x$ films are solid solutions, not a composite or a superlattice of ZnO and GaN. φ-scan plots of (1 0 –1 1) peaks confirm clear six-fold symmetry [Fig. 3(c)], indicating epitaxial growth below 100 °C, which is attributable to the high kinetic energy of laser-ablated species (over several eV) and enhanced ZnO and GaN surface migration [39,40] on atomically flat substrates. The crystallinity of the $(GaN)_{1-x}(ZnO)_x$ thin films

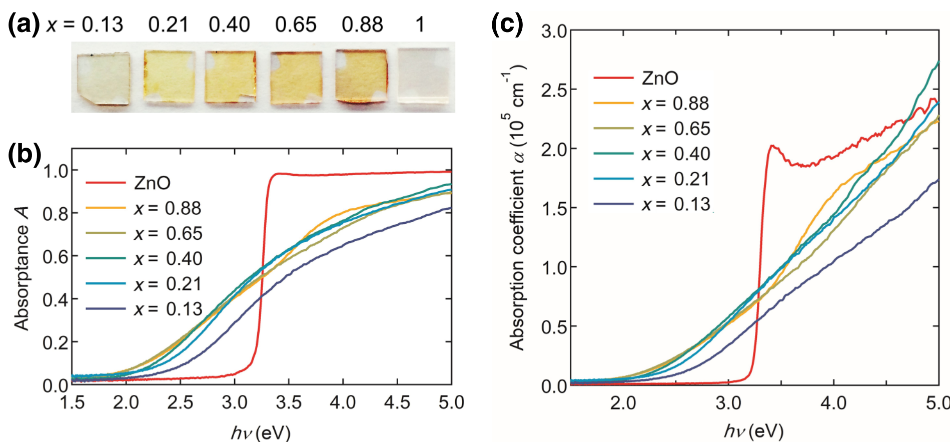

FIG. 4. (a) Photograph and (b) absorption spectra of $(GaN)_{1-x}(ZnO)_x$ thin films grown on Al_2O_3 substrates. (c) Absorption coefficients calculated from (b).

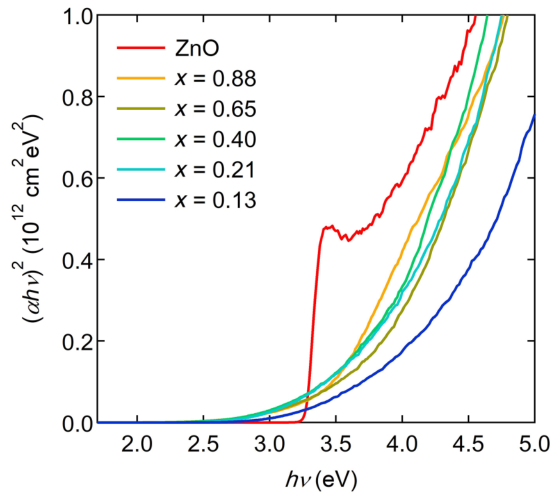

FIG. 5. Tauc plots of $(GaN)_{1-x}(ZnO)_x$ thin films grown on Al_2O_3 substrates, assuming a direct semiconductor model.

is improved on the ZnO substrate with better lattice matching, which is confirmed by the reduced peak width along the χ direction of the area detector [Fig. 3(d)].

B. Optical properties of solid-solution films

Figures 4(a) and 4(b), respectively, show a photograph and UV-visible absorption spectra of $(GaN)_{1-x}(ZnO)_x$ films grown on Al_2O_3 substrates. All of the films exhibit absorption edges around 2–2.5 eV. The absorption coefficients (α values) are on the order of 10^4 cm^{-1} [Fig. 4(c)], which agrees well with that previously reported for $(GaN)_{0.27}(ZnO)_{0.73}$ nanocrystals (4.6×10^4 cm^{-1} at 2.76 eV) [25]. Absorption spectra are also acquired for $(GaN)_{1-x}(ZnO)_x$ thin films grown on ZnO substrates. Those spectra almost coincide with those obtained from films on Al_2O_3 substrates (See Supplemental Material [24], Fig. S2). However, the ZnO substrate exhibits strong absorption in the UV (>3 eV); thus, only absorption spectra of films grown on Al_2O_3 substrates will be considered below.

Previous DRS spectral shape analyses using Tauc plot suggested that $(GaN)_{1-x}(ZnO)_x$ is a direct-transition semiconductor [10]. However, absorption spectra here exhibit poor agreement with Tauc plots that assume a direct transition with the form $(\alpha h\nu)^2 \propto (h\nu - E_g)$ (Fig. 5). A possible explanation for the discrepancy is that local structures,

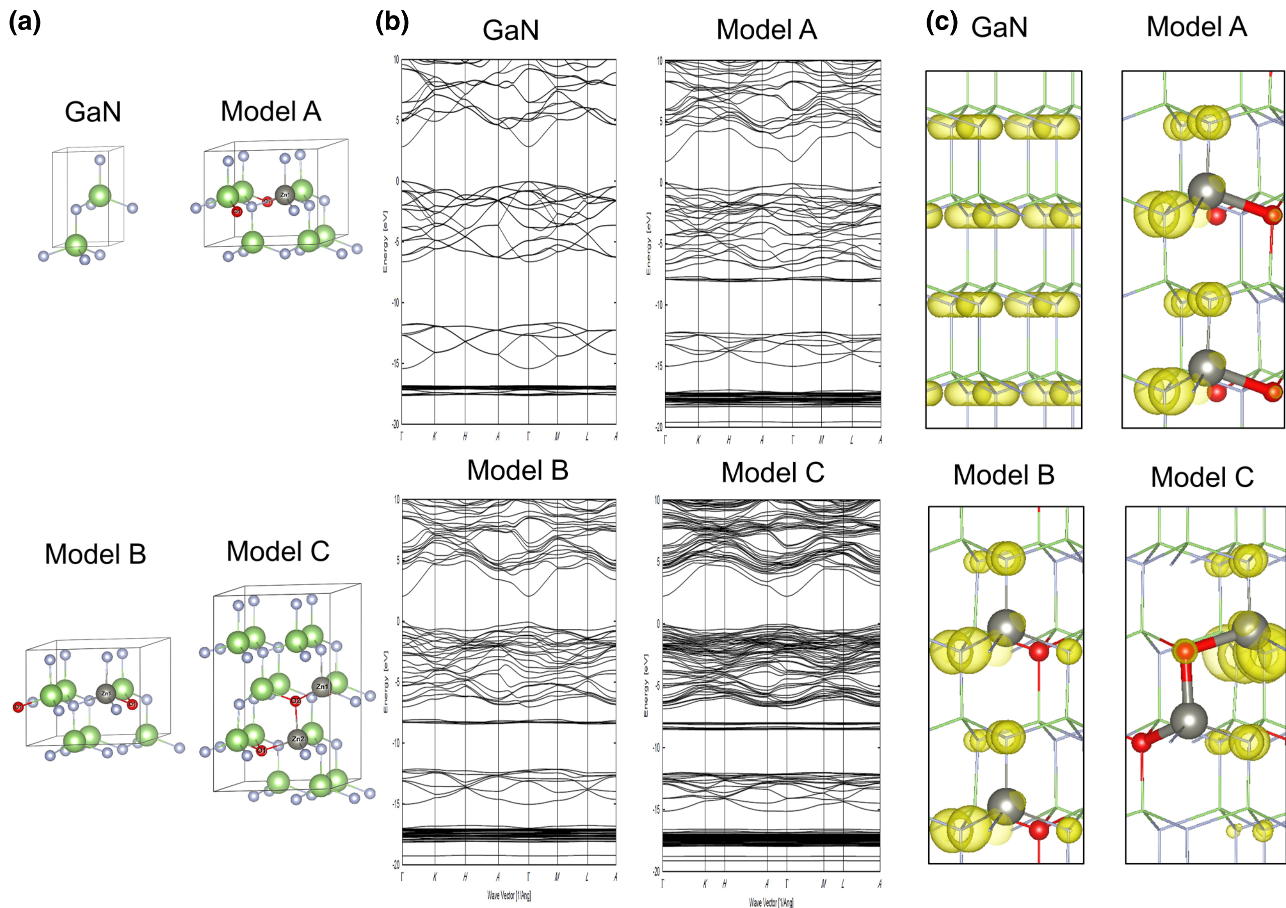

FIG. 6. (a) Optimized structures, (b) band dispersion diagrams, and (c) charge-density maps of GaN and the three model structures of $(GaN)_{0.75}(ZnO)_{0.25}$. Green, blue, gray, and red balls in (a) and (c) represent Ga, N, Zn, and O atoms, respectively.

such as the short-range order of Zn-O/Ga-N pairs, are different because of the lower synthesis temperature [31]. Another reason may have been spectral shape distortion in the previous study due to the strong optical absorption of samples that were associated with data conversion from diffuse reflectance to absorbance by the Kubelka-Munk method [32]. High absorbance enhances the intensity of regular light reflection if it is not sufficiently diluted with a white standard. The reflection causes a difference in scattering factor between sample and standard, resulting in an underestimation of α. The latter is supported by the shape of the absorption spectrum of a diluted colloidal solution of $(GaN)_{0.27}(ZnO)_{0.73}$ nanocrystals: It was also inconsistent with a direct-transition semiconductor model (see Supplemental Material [24], Fig. S3), although the spectral shape has not been analyzed in the original report [25].

Despite the deviation in spectral shape, our thin films and the colloidal solution [25] exhibit 10^4-cm^{-1} α values, which are comparable to those for conventional direct-transition semiconductors. It is known that Tauc plot analysis is invalid for the end members (GaN and ZnO) due to the strong contribution of exciton absorption. However, the solid-solution ($0 < x < 1$) films show broad and structureless absorption edges, indicating little contribution of exciton absorption. To investigate the origin of this inconsistency, we conduct first-principles calculations for $(GaN)_{1-x}(ZnO)_x$ ($x = 0$, 0.25, 0.75, and 1). For each solid solution ($x = 0.25$ or 0.75), three model structures of A, B, and C are prepared [Figs. 6(a) and 7(a)]: In model A, Zn (Ga) and O (N) form no Zn-O (Ga-N) pair in the ($2 \times 2 \times 1$) supercell of GaN (ZnO). In model B, Zn (Ga) and O (N) form a Zn-O (Ga-N) pair in the ($2 \times 2 \times 1$) supercell of GaN(ZnO). In model C, Zn (Ga) and O (N) form a Zn-O-Zn-O (Ga-N-Ga-N) chain in the ($2 \times 2 \times 2$) supercell of GaN(ZnO). Figure 6(b) shows the band dispersion diagrams of GaN and $(GaN)_{0.75}(ZnO)_{0.25}$. All three model structures of $(GaN)_{0.75}(ZnO)_{0.25}$ as well as GaN are direct-transition-type semiconductors. However, the $(GaN)_{0.75}(ZnO)_{0.25}$ model structures show a rather flat valence-band top and narrower band gap compared with GaN. The ZnO-rich $(GaN)_{0.25}(ZnO)_{0.75}$ model structures also show a flatter valence-band top and narrower band gap than ZnO [Fig. 7(b)]. We also calculate charge density maps of the valence-band maximum at Γ point

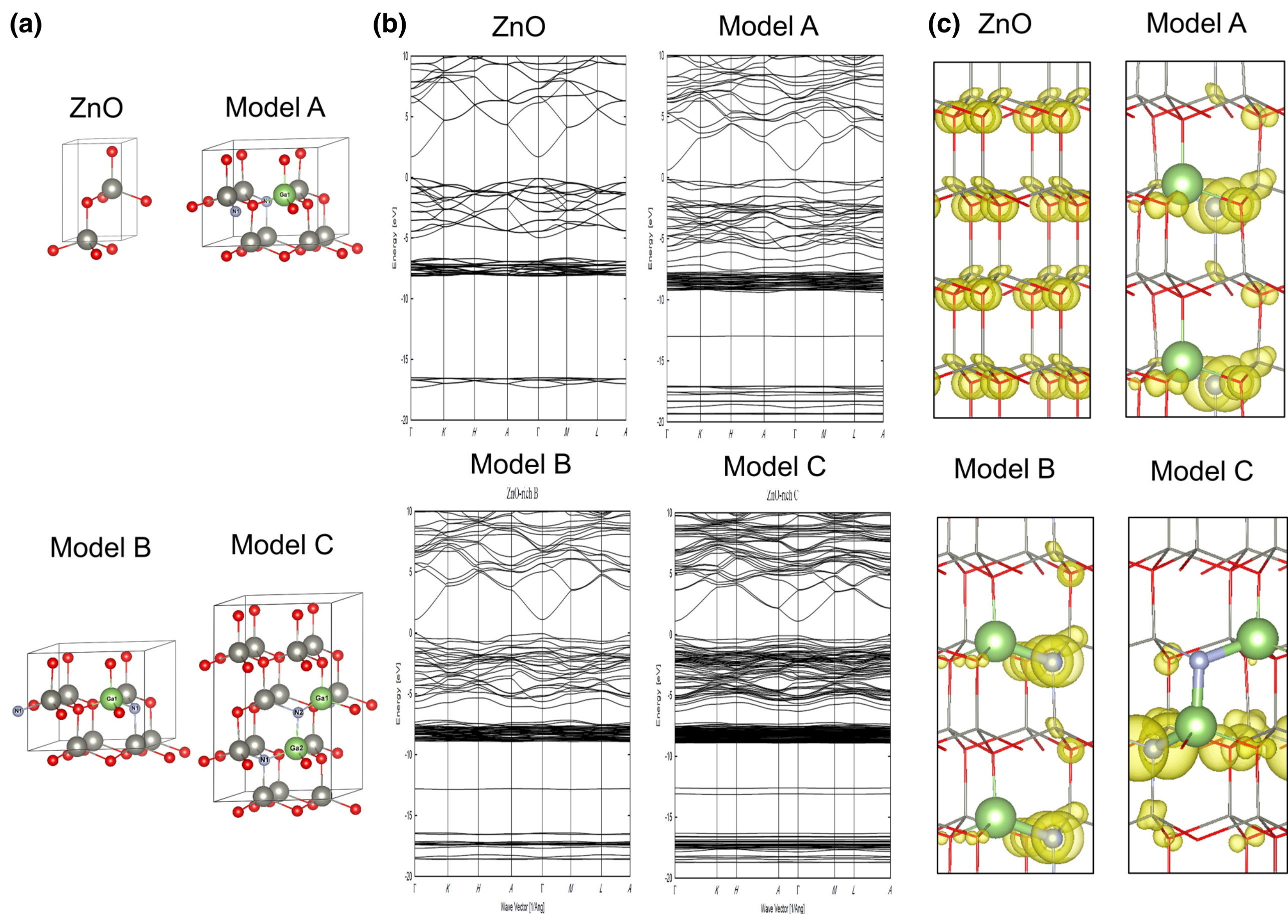

FIG. 7. (a) Optimized structures, (b) band dispersion diagrams, and (c) charge-density maps of ZnO and the three model structures of $(GaN)_{0.25}(ZnO)_{0.75}$. Green, blue, gray, and red balls in (a) and (c) represent Ga, N, Zn, and O atoms, respectively.

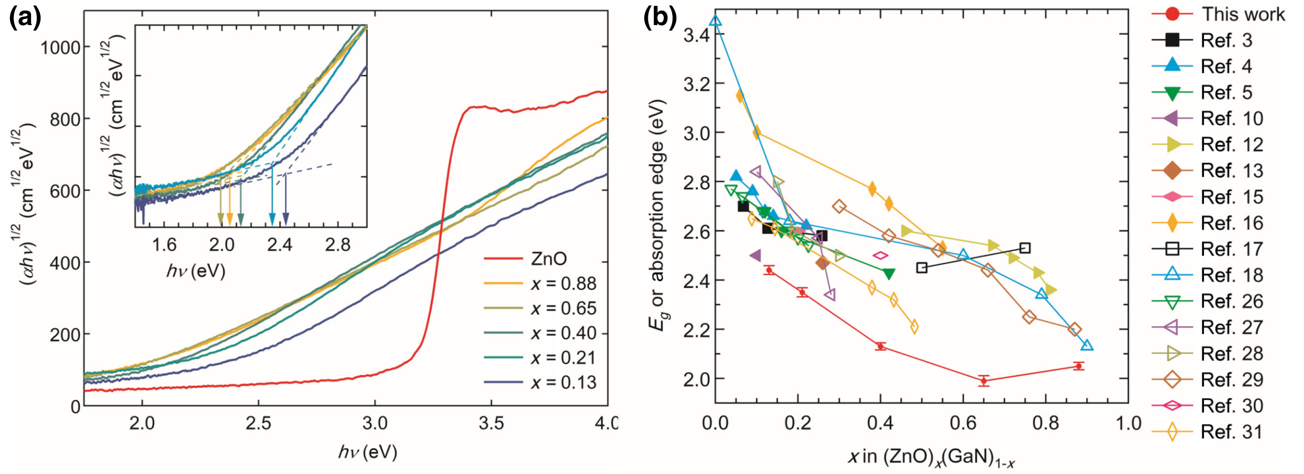

FIG. 8. (a) Tauc plots $[(\alpha h\nu)^{1/2}$ vs $(h\nu\text{-}E_g)]$ of the $(GaN)_{1-x}(ZnO)_x$ solid-solution thin films. Inset is the magnification around the absorption edges. (b) E_g of the $(GaN)_{1-x}(ZnO)_x$ solid-solution thin films vs x. Absorption edges reported in the literature are also plotted for reference. Markers connected with solid lines are taken from the same report.

[see Figs. 6(b) and 7(b)], since the flat band suggests that localization of the orbital causes nonparabolicity in band structure. Figures 6(c) and 7(c) indicate that the orbital of the valence-band maximum is localized on N atoms bonded with Zn in both $(GaN)_{0.75}(ZnO)_{0.25}$ and $(GaN)_{0.25}(ZnO)_{0.75}$. These results suggest that formation of Zn-N bonds is an origin of the deviation of the spectral shape from the Tauc plot, because the Tauc plot analysis assumes a parabolic shape for both conduction-band bottom and valence-band top.

Finally, we evaluate the compositional dependence of E_g of the $(GaN)_{1-x}(ZnO)_x$ thin films. Although the Tauc plot analysis does not have a clear physical basis for systems with a localized valence-band maximum as well as a highly disordered structure similar to heavily isoelectronically doped compound semiconductors [41], we practically use modified Tauc plots of $(\alpha h\nu)^{1/2} \propto (h\nu\text{-}E_g)$ for determining E_g because of their good linearity, as shown in Fig. 8(a). Figures 8(b) reveal an asymmetric downward bowing of E_g, where E_g decreases with increasing x, with a minimum of approximately 2.0 eV at $x = 0.65$. As mentioned above, the most GaN-rich film ($x = 0.13$) is relatively over-oxidized. It is reported that excess oxygen in GaN forms a shallow donor level [42], which might increase the E_g through band-gap renormalization and band filling effect as in the case of Si- or Ge-doped GaN [43]. However, in our most GaN-rich film, doped electrons are almost compensated probably due to formation of Ga vacancies and/or interstitial oxygens [44,45]: Its carrier concentration n_e, determined by Hall measurement, is 1.1×10^{19} cm^{-3}. Because the band-gap increase estimated from this n_e value is <60 meV [43], we believe that the influence of the excess oxygen on E_g is relatively small.

Asymmetric band bowing similar to our results was recently reported for synthesized $(GaN)_{1-x}(ZnO)_x$ powders and nanocrystals having wide compositional ranges [13,15,18]. Although the asymmetric E_g dependence on x was not entirely understood [8,19], it could be rationalized if the E_g reduction was more prominent in the ZnO-rich region relative to the GaN-rich region because of differences in the effective masses at the valence-band maximum and the conduction-band minimum [8]. Another speculation based on our theoretical calculation is that the reduction of E_g is caused by an increase of the Zn-N bond. Table I summarizes the E_g obtained from the calculation. In both the GaN-rich and the ZnO-rich solid solutions, E_g decreases in the order of models C, B, and A, where the number of Zn-N bonds increases in the same order. This tendency might suggest that formation of Zn-N bonds is kinetically more preferred in a ZnO-rich composition than in a GaN-rich one, although the absolute values of the E_g calculated in our study are inaccurate due to a well-known limitation of the LDA and exclusion of the

TABLE I. E_g of the GaN, ZnO, and $(GaN)_{1-x}(ZnO)_x$ solid solutions ($x = 0.25$ and 0.75) calculated from the band dispersion diagrams in Figs. 6(b) and 7(b).

		$(GaN)_{0.75}(ZnO)_{0.25}$				$(GaN)_{0.25}(ZnO)_{0.75}$		
Model	GaN	A	B	C	ZnO	A	B	C
Band gap (eV)	2.90	1.81	2.13	2.25	1.77	0.75	1.14	1.18

contribution of excitonic absorption. Further analyses of E_g and α, combined with theoretical calculations for more accurate evaluation of E_g , such as GW approximation with Bethe-Salpeter equation, are needed.

IV. CONCLUSION

Epitaxial $(GaN)_{1-x}(ZnO)_x$ thin films are synthesized with multitarget PLD synchronized with a process gas supply control system. The single-phase $(GaN)_{1-x}(ZnO)_x$ solid-solution films are obtained by reducing the thickness of a GaN/ZnO pair in the GaN/ZnO superlattices to approximately 1 nm due to interlayer mixing. Low-temperature epitaxial growth enables a wide-range compositional synthesis of the solid-solution thin films. The solid-solution thin films have large absorption coefficients ($>10^4$ cm^{-1}) in the visible-light region. The shapes of the absorption edges are inconsistent with a direct band gap. First-principles calculation suggests that this inconsistency originates from localization of the valence-band maximum on N atoms bonded with Zn. The energy gap of the $(GaN)_{1-x}(ZnO)_x$ solid solutions empirically determined by modified Tauc plot exhibits asymmetric bowing with an approximately 2.0-eV minimum at $x = 0.65$. These results demonstrate that low-temperature epitaxial growth is an effective synthesis of $(GaN)_{1-x}(ZnO)_x$ solid solutions with controlled chemical composition. This enables a systematic study of fundamental physical properties. Although beyond the scope of this study, the fabricated GaN/ZnO superlattices could be useful for optoelectronic applications.

ACKNOWLEDGMENTS

We thank Dr. Shoichiro Nakao for his assistance with optical measurements. This study was in part supported by CREST, Japan Science and Technology Agency (JST) (Grant No. JPMJCR12C4) and the Grant-in-Aid for Scientific Research on Innovation Areas "Mixed anion" (Grants No. JP16H06438 and No. JP16H06441) from the Japan Society for the Promotion of Science (JSPS). C. Yang acknowledges funding support from Deutsche Forschungsgemeinschaft (Grant No. YA 511/1-1).

[1] A. J. Bard and M. A. Fox, Artificial photosynthesis: Solar splitting of water to hydrogen and oxygen, Acc. Chem. Res. **28**, 141 (1995).

[2] A. Fujishima and K. Honda, Electrochemical photolysis of water at a semiconductor electrode, Nature **238**, 37 (1972).

[3] K. Maeda, T. Takata, M. Hara, N. Saito, Y. Inoue, H. Kobayashi, and K. Domen, GaN:ZnO solid solution as a photocatalyst for visible-light-driven overall water splitting, J. Am. Chem. Soc. **127**, 8286 (2005).

[4] K. Maeda, K. Teramura, T. Takata, M. Hara, N. Saito, K. Toda, Y. Inoue, H. Kobayashi, and K. Domen, Overall water splitting on $(Ga_{1-x}Znx)(N_{1-x}O_x)$ solid solution photocatalyst: Relationship between physical properties and photocatalytic activity, J. Phys. Chem. B **109**, 20504 (2005).

[5] K. Maeda, K. Teramura, D. L. Lu, T. Takata, N. Saito, Y. Inoue, and K. Domen, Photocatalyst releasing hydrogen from water, Nature **440**, 295 (2006).

[6] K. Maeda and K. Domen, New non-oxide photocatalysts designed for overall water splitting under visible light, J. Phys. Chem. C **111**, 7851 (2007).

[7] S. Z. Wang and L. W. Wang, Atomic and Electronic Structures of GaN/ZnO Alloys, Phys. Rev. Lett. **104**, 065501 (2010).

[8] M. N. Huda, Y. F. Yan, S. H. Wei, and M. M. Al-Jassim, Electronic structure of ZnO:GaN compounds: Asymmetric bandgap engineering, Phys. Rev. B **78**, 195204 (2008).

[9] H. Pan and Y. W. Zhang, GaN/ZnO superlattice nanowires as photocatalyst for hydrogen generation: A first-principles study on electronic and magnetic properties, Nano Energ. **1**, 488 (2012).

[10] A. A. Reinert, C. Payne, L. M. Wang, J. Ciston, Y. M. Zhu, and P. G. Khalifah, Synthesis and characterization of visible light absorbing $(GaN)_{1-x}(ZnO)_x$ semiconductor nanorods, Inorg. Chem. **52**, 8389 (2013).

[11] K. Maeda and K. Domen, Solid solution of GaN and ZnO as a stable photocatalyst for overall water splitting under visible light, Chem. Mater. **22**, 612 (2010).

[12] S. C. Yan, Z. Q. Wang, Z. S. Li, and Z. G. Zou, Two-step reactive template route to a mesoporous ZnGaNO solid solution for improved photocatalytic performance, J. Mater. Chem. **21**, 5682 (2011).

[13] J. P. Wang, B. B. Huang, Z. Y. Wang, P. Wang, H. F. Cheng, Z. K. Zheng, X. Y. Qin, X. Y. Zhang, Y. Dai, and M.-H. Whangbo, Facile synthesis of Zn-rich $(GaN)_{1-x}(ZnO)_x$ solid solutions using layered double hydroxides as precursors, J. Mater. Chem. **21**, 4562 (2011).

[14] M. Mapa, K. S. Thushara, B. Saha, P. Chakraborty, C. M. Janet, R. P. Viswanath, C. M. Nair, K. V. G. K. Murty, and C. S. Gopinath, Electronic structure and catalytic study of solid solution of GaN in ZnO, Chem. Mater. **21**, 2973 (2009).

[15] K. Lee, B. M. Tienes, M. B. Wilker, K. J. Schnitzenbaumer, and G. Dukovic, $(Ga_{1-x}Zn_x)(N_{1-x}O_x)$ nanocrystals: Visible absorbers with tunable composition and absorption spectra, Nano Lett. **12**, 3268 (2012).

[16] M. Zhong, Y. H. Ma, P. Oleynikov, K. Domen, and J. J. Delaunay, A conductive ZnO–ZnGaON nanowire-array-on-a-film photoanode for stable and efficient sunlight water splitting, Energ. Environ. Sci. **7**, 1693 (2014).

[17] M. Yang, Q. Huang, and X. Q. Jin, Microwave synthesis of porous ZnGaNO solid solution for improved visible light photocatalytic performance, Solid State Sci. **14**, 465 (2012).

[18] Y. G. Li, L. P. Zhu, Y. F. Yang, H. Song, Z. R. Lou, Y. M. Guo, and Z. Z. Ye, A full compositional range for a $(Ga_{1-x}Zn_x)(N_{1-x}O_x)$ nanostructure: High efficiency for overall water splitting and optical properties, Small **11**, 871 (2015).

[19] L. L. Jensen, J. T. Muckerman, and M. D. Newton, First-principles studies of the structural and electronic properties of the $(Ga_{1-x}Zn_x)(N_{1-x}O_x)$ solid solution photocatalyst, J. Phys. Chem. C **112**, 3439 (2008).

[20] W. Wei, Y. Dai, K. S. Yang, M. Guo, and B. B. Huang, Origin of the visible light absorption of GaN-rich $Ga_{1-x}Zn_xN_{1-x}O_x$ ($x = 0.125$) solid solution, J. Phys. Chem. C **112**, 15915 (2008).

[21] T. Hirai, K. Maeda, M. Yoshida, J. Kubota, S. Ikeda, M. Matsumura, and K. Domen, Origin of visible light absorption in GaN-rich $(Ga_{1-x}Zn_x)(N_{1-x}O_x)$ photocatalysts, J. Phys. Chem. C **111**, 18853 (2007).

[22] M. Yoshida, T. Hirai, K. Maeda, N. Saito, J. Kubota, H. Kobayashi, Y. Inoue, and K. Domen, Photoluminescence spectroscopic and computational investigation of the origin of the visible light response of $(Ga_{1-x}Zn_x)(N_{1-x}O_x)$ photocatalyst for overall water splitting, J. Phys. Chem. C **114**, 15510 (2010).

[23] E. J. McDermott, E. Z. Kurmaev, T. D. Boyko, L. D. Finkelstein, R. J. Green, K. Maeda, K. Domen, and A. Moewes, Structural and band gap investigation of GaN:ZnO heterojunction solid solution photocatalyst probed by soft X-ray spectroscopy, J. Phys. Chem. C **116**, 7694 (2012).

[24] See Supplemental Material at http://link.aps.org/supplemental/10.1103/PhysRevApplied.10.044001, which includes Refs. [3-5,10,12,13,15-18, 26-31]. Table S1 gives further details on the thicknesses of the GaN/ZnO pairs, the absorption edges of $(GaN)_{1-x}(ZnO)_x$ reported in the literatures are sumerized in FIG. S1, the absorption spectrum of $(GaN)_{1-x}(ZnO)_x$ thin films grown on ZnO substrates is shown in FIG. S2, and more information on the absorption spectrum and Tauc plots of a diluted colloidal solution of $(GaN)_{0.27}(ZnO)_{0.73}$ nanocrystals is provided in FIG. S3.

[25] C. H. Chuang, Y. G. Lu, K. Lee, J. Ciston, and G. Dukovic, Strong visible absorption and broad time scale excited-state relaxation in $(Ga_{1-x}Zn_x)(N_{1-x}O_x)$ nanocrystals, J. Am. Chem. Soc. **137**, 6452 (2015).

[26] X. Sun, K. Maeda, M. Le Faucheur, K. Teramura, and K. Domen, Preparation of $(Ga_{1-x}Zn_x)$ $(N_{1-x}O_x)$ solid-solution from $ZnGa_2O_4$ and ZnO as a photo-catalyst for overall water splitting under visible light, Appl. Catal. A Gen. **327**, 114 (2007).

[27] H. Chen, W. Wen, Q. Wang, J. C. Hanson, J. T. Muckerman, E. Fujita, A. I. Frenkel, and J. A. Rodriguez, Preparation of $(Ga_{1-x}Zn_x)(N_{1-x}O_x)$ photocatalysts from the reaction of NH_3 with Ga_2O_3/ZnO and $ZnGa_2O_4$: In situ time-resolved XRD and XAFS studies, J. Phys. Chem. C **113**, 3650 (2009).

[28] H. Hashiguchi, K. Maeda, R. Abe, A. Ishikawa, J. Kubota, and K. Domen, Photoresponse of GaN:ZnO electrode on FTO under visible light irradiation, Bull. Chem. Soc. Jpn. **82**, 401 (2009).

[29] W. Q. Han, Z. X. Liu, and H. G. Yu, Synthesis and optical properties of GaN/ZnO solid solution nanocrystals, Appl. Phys. Lett. **96**, 183112 (2010).

[30] W. Q. Han, Y. Zhang, C. Y. Nam, C. T. Black, and E. E. Mendez, Growth and electronic properties of GaN/ZnO solid solution nanowires, Appl. Phys. Lett. **97**, 083108 (2010).

[31] H. Y. Chen, L. P. Wang, J. M. Bai, J. C. Hanson, J. B. Warren, J. T. Muckerman, E. Fujita, and J. A. Rodriguez, In situ XRD studies of ZnO/GaN mixtures at high pressure and high temperature: Synthesis of Zn-rich $(Ga_{1-x}Zn_x)(N_{1-x}O_x)$ photocatalysts, J. Phys. Chem. C **114**, 1809 (2010).

[32] G. Kortüm, W. Braun, and G. Herzog, Principles and techniques of diffuse-reflectance spectroscopy, Angew. Chem. Int. Ed. Engl. **2**, 333 (1963).

[33] S. Shet, Y. F. Yan, N. Ravindra, J. Turner, and M. Al-Jassim, Photoelectrochemical behavior of mixed ZnO and GaN (ZnO:GaN) thin films prepared by sputtering technique, Appl. Surf. Sci. **270**, 718 (2013).

[34] S. Shet, Y. F. Yan, J. Turner, and M. Al-Jassim, Effect of gas ambient and varying RF sputtering power for bandgap narrowing of mixed (ZnO:GaN) thin films for solar driven hydrogen production, J. Power Sources **232**, 74 (2013).

[35] D. Drouin, A. R. Couture, D. Joly, X. Tastet, V. Aimez, and R. Gauvin, CASINO V2.42: A fast and easy-to-use modeling tool for scanning electron microscopy and microanalysis users, Scanning **29**, 92 (2007).

[36] G. Kresse and J. Furthmüller, Efficient iterative schemes for *ab initio* total-energy calculations using a plane-wave basis set, Phys. Rev. B **54**, 11169 (1996).

[37] P. E. Blochl, Projector augmented-wave method, Phys. Rev. B **50**, 17953 (1994).

[38] J. P. Perdew and A. Zunger, Self-interaction correction to density-functional approximations for many-electron systems, Phys. Rev. B **23**, 5048 (1981).

[39] A. Kobayashi, H. Fujioka, J. Ohta, and M. Oshima, Room temperature layer by layer growth of GaN on atomically flat ZnO, Jpn. J. Appl. Phys. **43**, L53 (2004).

[40] A. Sasaki, W. H. A. Matsuda, N. Tateda, S. Otaka, S. Akiba, K. Saito, T. Yodo, and M. Yoshimoto, Buffer-enhanced room-temperature growth and characterization of epitaxial ZnO thin films, Appl. Phys. Lett. **86**, 231911 (2005).

[41] Y. Zhang, B. Fluegel, A. Mascarenhas, H. P. Xin, and C. W. Tu, Optical transitions in the isoelectronically doped semiconductor GaP:N: An evolution from isolated centers, pairs, and clusters to an impurity band, Phys. Rev. B **62**, 4493 (2000).

[42] H. Wang and A.-B. Chen, Calculation of shallow donor levels in GaN, J. Appl. Phys. **87**, 7859 (2000).

[43] M. Feneberg, S. Osterburg, K. Lange, C. Lidig, B. Garke, R. Goldhahn, E. Richter, C. Netzel, M. D. Neumann, N. Esser, S. Fritze, H. Witte, J. Bläsing, A. Dadgar, and A. Krost, Band gap renormalization and Burstein-Moss effect in silicon- and germanium-doped wurtzite GaN up to 10^{20} cm^{-3}, Phys. Rev. B **90**, 075203 (2014).

[44] J. Oila, V. Ranki, J. Kivioja, K. Saarinen, P. Hautojärvi, J. Likonen, J. M. Baranowski, K. Pakula, T. Suski, M. Leszczynski, and I. Grzegory, Influence of dopants and substrate material on the formation of Ga vacancies in epitaxial GaN layers, Phys. Rev. B **63**, 045205 (2001).

[45] A. F. Wright, Substitutional and interstitial oxygen in wurtzite GaN, J. Appl. Phys. **98**, 103531 (2005).